Bias in low-multipole cosmic microwave background reconstructions

Craig J. Copi,[1]★ Dragan Huterer,[2]★ Dominik J. Schwarz[3]★ and Glenn D. Starkman[1]★

[1]*CERCA/Department of Physics/ISO, Case Western Reserve University, Cleveland, OH 44106-7079, USA*
[2]*Department of Physics, University of Michigan, 450 Church Street, Ann Arbor, MI 48109-1040, USA*
[3]*Fakultät für Physik, Universität Bielefeld, Postfach 100131, 33501 Bielefeld, Germany*

ABSTRACT

The large-angle, low-multipole cosmic microwave background (CMB) provides a unique view of the largest angular scales in the Universe. Study of these scales is hampered by the facts that we have only one Universe to observe, only a few independent samples of the underlying statistical distribution of these modes, and an incomplete sky to observe due to the interposing Galaxy. Techniques for reconstructing a full sky from partial-sky data are well known and have been applied to the large angular scales. In this work, we critically study the reconstruction process and show that, in practice, the reconstruction is biased due to leakage of information from the region obscured by foregrounds to the region used for the reconstruction. We conclude that, despite being suboptimal in a technical sense, using the unobscured region without reconstructing is the most robust measure of the true CMB sky. We also show that for noise-free data reconstructing using the usual optimal, unbiased estimator may be employed without smoothing, thus avoiding the leakage problem. Unfortunately, directly applying this to real data with noise and residual, unmasked foregrounds yields highly biased reconstructions requiring further care to apply this method successfully to the real-world CMB.

Key words: cosmic background radiation – large-scale structure of Universe.

1 INTRODUCTION

Several prominent anomalies in the large-angle, low-ℓ cosmic microwave background (CMB) have been identified, starting with pioneering observations by the *Cosmic Background Explorer* (*COBE*; Bennett et al. 1996), and confirmed and extended with the high-precision observations from the *Wilkinson Microwave Anisotropy Probe* (*WMAP*; Bennett et al. 2003). These anomalies include the unexpectedly low correlations at scales above 60° (Bennett et al. 1996, 2003; Copi et al. 2010; Sarkar et al. 2011), the alignments of the largest multipoles with each other and the Solar system (de Oliveira-Costa et al. 2004; Schwarz et al. 2004; Land & Magueijo 2005; Copi et al. 2006), a parity asymmetry at low multipoles (Kim & Naselsky 2010a,b,d,c) and the spatial asymmetries in the distribution of power observed at smaller scales (Eriksen et al. 2004a,b; Hansen et al. 2009). Numerous attempts have been made to explain or explain away these anomalies (Slosar & Seljak 2004; Hajian 2007; Afshordi, Geshnizjani & Khoury 2009; Bennett et al. 2011) – none of them successful (for a review see Copi et al. 2010, and references therein).

The most peculiar and robust CMB anomaly is arguably the lack of correlation on large angular scales first observed by *COBE*

(Bennett et al. 1996) and confirmed and further quantified through the $S_{1/2}$ statistic by *WMAP* (Spergel et al. 2003). Subsequent study of the two-point angular correlation function, $C(\theta)$, has found further oddities; the large-angle correlation is mainly missing outside of the Galactic region, there being essentially no correlation on large angles. The large-angle correlation that is observed comes from the foreground-removed Galactic region of the reconstructed full-sky map (Copi et al. 2009). From the internal linear combination (ILC) map,[1] the full-sky map created from the individual frequency bands which provides our best picture of the full-sky microwave background radiation, it is found that the lack of correlation is unlikely at the approximately 95 per cent level. However, when solely the region outside the Galaxy of the individual frequency or ILC maps are analysed, the lack of correlation is rare at the approximately 99.975 per cent level (Copi et al. 2009).

The study of the large-angle CMB presents special problems that must be treated carefully. Since there is only one Universe to observe and a few independent modes at low ℓ, large sky coverage is needed, and even with this coverage, very little independent information about the ensemble is available. Further, given the observed low quadrupole power, $C_2^{\mathrm{obs}} \sim 100$–$200\,(\mu\mathrm{K})^2$, compared to the best-fitting Λ cold dark matter (ΛCDM) model, $C_2^{\Lambda\mathrm{CDM}} \sim 1300\,(\mu\mathrm{K})^2$,

---

[1] The ILC map and all data from the *WMAP* mission are freely available online at http://lambda.gsfc.nasa.gov/.

large-angle studies are particularly sensitive to assumptions and unintended biases.

One suggestive example of this is provided by the ILC map itself. If we use a pixel-based estimator for the C_ℓ as implemented in SPICE (Chon et al. 2004), we can easily determine the quadrupole power inside and outside the *WMAP*-provided analysis mask KQ75y7 to be

$$C_2^{\text{inside}} \approx 610\,(\mu\text{K})^2, \qquad C_2^{\text{outside}} \approx 80\,(\mu\text{K})^2. \tag{1}$$

The KQ75y7 mask cuts out approximately 25 per cent of the sky. Taking the weighted average of these values produces the intriguing result

$$0.25 C_2^{\text{inside}} + 0.75 C_2^{\text{outside}} \approx 200\,(\mu\text{K})^2, \tag{2}$$

a value consistent with the *WMAP*-reported C_2 (Larson et al. 2011). Again, we stress that this is a suggestive example, not a careful analysis; the pseudo-C_ℓ (PCL) estimator employed here is suboptimal, we have not included errors on the estimates, etc. It does, however, show the wide discrepancy between the Galactic region and the rest of the sky, a common theme for the ILC map. Further, it shows how a large value mixed in from a small region of the sky significantly impacts the final result.

In a recent paper (Efstathiou, Ma & Hanson 2010), the authors claimed that the low $S_{1/2}$ results are due to the use of a suboptimal estimator (the pixel-based estimator) of $C(\theta)$ and proposed an alternative based on reconstructing the full sky. This proposal avoids addressing the question of *why* the partial sky contains essentially no correlations on large angular scales and instead focuses on a new question that centres on the issue of how the full sky is reconstructed. In this work, we carefully study full-sky reconstruction algorithms and their effects on the low-ℓ CMB.

It is well known that contamination affects the reconstruction of the low multipoles (Bielewicz, Górski & Banday 2004; Naselsky, Verkhodanov & Nielsen 2008; Liu & Li 2009; Aurich & Lustig 2011). In particular, Aurich & Lustig (2011) have found that smoothing of full-sky map prior to analysis, as required by a reconstruction algorithm (see Efstathiou et al. 2010, and our discussion below), leaks information from the region inside the mask to pixels outside the mask. They showed that the pixels outside the mask have errors that are a significant fraction of the mean CMB temperature. They further find that it is safest to calculate the two-point angular correlation function on the cut sky. Here we confirm and extend these results.

Alternative analyses, such as that suggested in Efstathiou et al. (2010), must be performed with care. In this work, we carefully study the full-sky reconstruction, based on the cut-sky data, in a Universe with low quadrupole power. In Section 2, we briefly present the formalism typically employed in CMB studies. Section 3 contains our results, and we conclude in Section 4. Ultimately, we find that if a full-sky map, such as the ILC, is a faithful representation of the true CMB sky, then a reconstruction algorithm can reproduce its properties. This is not surprising: if the full-sky map is already trusted, there is no need to perform a reconstruction and nothing is gained by doing so. However, if part of the full sky is not trusted or is known to be contaminated, then, by reconstructing without properly accounting for the assumptions implicit in the algorithm, the final results will be biased towards the full-sky values. Again, this is not surprising; if information from the questioned region is allowed to leak into the rest of the map, then it will affect the final results and nothing will be learned about the validity of the reconstruction.

In any reconstruction of unknown values from the properties of existing data, assumptions must be made. Often these assumptions are not explicitly stated. For the work presented here, we take the observed microwave sky outside of the Galactic region as defined through the KQ75y7 mask to be a fair sample of the CMB. This partial-sky region is known to have essentially no correlations on large angular scales; it is unlikely in the best-fitting ΛCDM model at the 99.975 per cent level (Copi et al. 2009). Our study shows the bias introduced into full-sky reconstructions when an admixture of a region with larger angular correlations is included prior to reconstruction. We stress that results of the partial-sky analysis are *not* being questioned, instead a new question is being asked: how should the full sky be reconstructed when there is a wide disparity between the statistical properties of the region outside the Galaxy and that inside?

2 RECONSTRUCTION FORMALISM

Optimal, unbiased estimators for both the C_ℓ and $a_{\ell m}$ are well known and discussed extensively in the literature (see, for example, Tegmark 1997; Efstathiou 2004; de Oliveira-Costa & Tegmark 2006; Efstathiou et al. 2010). Here we provide a brief overview of the maximum likelihood estimator (MLE) technique and introduce our notation. For details including discussions of invertibility of the matrices, proofs of optimality, etc., see the references.

The microwave temperature fluctuations on the sky can be represented by the vector $x(\hat{e}_j)$,

$$x = \mathbf{Y}a + n, \tag{3}$$

where $\mathbf{Y}$ is the matrix of the $Y_{\ell,m}(\hat{e}_j)$, j runs over all pixels on the sky, $\hat{e}_j$ is the radial unit vector in the direction of pixel j, a is the vector of $a_{\ell m}$ coefficients and n is the noise in each pixel. For the work considered here, we are only interested in the large-angle, low-ℓ behaviour, so we assume that n can be ignored and set $n = 0$ in what follows. When working with the *WMAP* data at low resolution, this is justified; for example, the W-band maps at $N_{\text{side}} = 16$ have pixel noise $\sigma_{\text{pix}} < 3\,\mu\text{K}$. At higher resolution this is not as clearly justified. In this work we study reconstruction bias independent of pixel noise, so we may ignore n for our simulations. When setting $n = 0$, we are further assuming that the region we are analysing is free of foregrounds. This is a standard, though implicit, assumption when reconstructions are performed. The covariance matrix is then given by

$$\mathbf{C} = \langle x x^{\mathrm{T}} \rangle = \mathbf{S}. \tag{4}$$

Here the angle brackets, $\langle \cdot \rangle$, represent an ensemble average. This is the expectation value of the theoretical two-point angular correlation function, not its measured value. As is customary, we call $\mathbf{S}$ the signal matrix despite the fact that it is *not* the two-point angular correlation measured on the sky. We do not include a noise matrix, $\mathbf{N}$, in our covariance since we are neglecting noise.

2.1 Reconstructing the $a_{\ell m}$

To reconstruct the $a_{\ell m}$, we define the signal matrix as the two-point angular correlation function of *the unreconstructed modes*:

$$\mathbf{C} = \mathbf{S} = \sum_{\ell=\ell_{\text{recon}}+1}^{\ell_{\text{max}}} C_\ell \mathbf{P}^\ell. \tag{5}$$

Here $\mathbf{P}^\ell$ is the matrix of the weighted Legendre polynomials,

$$\mathbf{P}^\ell_{i,j} \equiv \frac{2\ell+1}{4\pi} P_\ell(\hat{e}_i \cdot \hat{e}_j), \tag{6}$$

and we assume that all modes with $2 \leq \ell \leq \ell_{\mathrm{recon}}$ are to be reconstructed. Here ℓ_{max} is the maximum multipole considered. We have chosen $\ell_{\mathrm{max}} = 4N_{\mathrm{side}} + 2$ for this work. The optimal, unbiased estimator is then given by (de Oliveira-Costa & Tegmark 2006)

$$\hat{a} = \mathbf{W}x, \qquad \mathbf{W} \equiv [\mathbf{Y}^{\mathrm{T}}\mathbf{C}^{-1}\mathbf{Y}]^{-1}\mathbf{Y}^{\mathrm{T}}\mathbf{C}^{-1}. \tag{7}$$

Note that here and throughout we work in the real spherical harmonic basis, so $\mathbf{Y}$ is a real matrix. The covariance matrix of our estimator is

$$\Sigma \equiv \langle \hat{a}\hat{a}^{\mathrm{T}} \rangle - \langle \hat{a} \rangle \langle \hat{a} \rangle^{\mathrm{T}} = [\mathbf{Y}^{\mathrm{T}}\mathbf{C}^{-1}\mathbf{Y}]^{-1}. \tag{8}$$

The signal matrix, $\mathbf{C}$, need not include all pairs of pixels on the sky. When it does, a reconstruction will produce precisely the spherical harmonic decomposition. Conversely, when a sky is masked, we only include the unmasked pixels in $\mathbf{C}$. The process of 'masking' is thus performed by removing the masked pixels from the signal matrix, and this process is equivalent to assigning infinite noise to the masked pixels.

2.2 Reconstructing the C_ℓ

To reconstruct the C_ℓ, we define the signal matrix as the two-point angular correlation of *all the modes*:

$$\mathbf{C} = \mathbf{S} = \sum_{\ell=2}^{\ell_{\mathrm{max}}} C_\ell \mathbf{P}^\ell. \tag{9}$$

Note that this differs from our previous definition (5). The optimal, unbiased estimator for the C_ℓ is then constructed from an unnormalized estimator, y_ℓ. Let

$$y_\ell \equiv x^{\mathrm{T}}\mathbf{E}^\ell x, \qquad \mathbf{E}^\ell \equiv \frac{1}{2}\mathbf{C}^{-1}\mathbf{P}^\ell\mathbf{C}^{-1}. \tag{10}$$

The correlation matrix of this estimator is the Fisher matrix,

$$\mathbf{F}_{\ell,\ell'} = \langle y_\ell y_{\ell'}^{\mathrm{T}} \rangle - \langle y_\ell \rangle \langle y_{\ell'} \rangle^{\mathrm{T}} = \frac{1}{2}\,\mathrm{Tr}[\mathbf{C}^{-1}\mathbf{P}^\ell\mathbf{C}^{-1}\mathbf{P}^{\ell'}]. \tag{11}$$

Finally, this gives the optimal, unbiased estimator of the C_ℓ:

$$\hat{C}_\ell = \sum_{\ell'} \mathbf{F}_{\ell,\ell'}^{-1} y_{\ell'}. \tag{12}$$

Though the full Fisher matrix can be calculated, it turns out to be nearly diagonal for reasonably small masks such as the *WMAP* KQ75y7 mask. In this case, the approximations

$$\mathbf{F}_{\ell,\ell'} \approx \frac{2\ell+1}{2\hat{C}_\ell^2}\delta_{\ell,\ell'}, \qquad \mathbf{F}_{\ell,\ell'}^{-1} \approx \frac{2\hat{C}_\ell^2}{2\ell+1}\delta_{\ell,\ell'} \tag{13}$$

may be employed. We have confirmed the validity of this approximation and have employed it when applicable in our subsequent analyses.

2.3 Relating the estimators

The optimal, unbiased estimators for $a_{\ell m}$ and C_ℓ are related to each other. If we define the weighted harmonic coefficients by

$$\beta \equiv \Sigma^{-1}\hat{a}, \tag{14}$$

then

$$y_\ell = \frac{1}{2}\sum_m |\beta_{\ell m}|^2 \tag{15}$$

is identical to (10) from which we may calculate $\hat{C}_\ell$ (de Oliveira-Costa & Tegmark 2006; Efstathiou et al. 2010).

In our discussion we have been careful to note that $\mathbf{C}$ is defined differently when used as an estimator for the $a_{\ell m}$ versus the C_ℓ. In practice, when the signal-to-noise ratio is large, the estimator for the $a_{\ell m}$ is not sensitive to the precise values and range of the C_ℓ employed. However, to find $\hat{C}_\ell$ from $\hat{a}$ through the weighted harmonic coefficients (14), the *full* signal matrix (9) must be used when calculating the covariance matrix (8) and Fisher matrix (11).

The above discussion shows that equation (12) is the optimal, unbiased estimator for the C_ℓ. Even so, given $\hat{a}$ from (7) it is tempting to define a naive estimator for the C_ℓ via

$$C_\ell^{\mathrm{e}} \equiv \frac{1}{2\ell+1}\sum_m |\hat{a}_{\ell m}|^2 \tag{16}$$

and use this to reconstruct $C(\theta)$ (see fig. 5 of Efstathiou et al. 2010). In general, this is a poor definition for the estimator as clearly an optimal, unbiased estimator for some quantity does *not* provide an optimal, unbiased estimator for the square of that quantity. Its use leads to a biased estimator for the C_ℓ and a biased reconstruction of $C(\theta)$. We will explore both this estimator and the optimal, unbiased one below.

2.4 Two-point angular correlation function

The two-point angular correlation function is defined as a sky average, that is by a sum over all pixels on the sky separated by the angle $\cos\theta_{i,j} = \hat{e}_i \cdot \hat{e}_j$:

$$C(\theta_{i,j}) \equiv \sum_{i,j} x_i x_j. \tag{17}$$

Ideally, the two-point angular correlation function would also contain an ensemble average over realizations of the underlying model. Since we only have one Universe, this ensemble average cannot be calculated. However, for a statistically isotropic Universe, the sky average and ensemble average are equivalent. This definition has the additional benefit that it can be calculated on a fraction of the sky.

Alternatively, the two-point angular correlation function may be expanded in a Legendre series,

$$C(\theta_{i,j}) = \sum_\ell \frac{2\ell+1}{4\pi} C_\ell P_\ell(\cos\theta_{i,j}). \tag{18}$$

Note that for partial-sky coverage or lack of statistical isotropy the C_ℓ in this expression are *not* the same as the $\hat{C}_\ell$ obtained from the $a_{\ell m}$ (see Copi et al. 2007, for a discussion). This subtlety will not be important for the following work.

2.5 $S_{1/2}$ statistic

To quantify the lack of large-angle correlations, the $S_{1/2}$ statistic has been defined by Spergel et al. (2003) to be

$$S_{1/2} \equiv \int_{-1/2}^{1} [C(\theta)]^2 \, \mathrm{d}(\cos\theta). \tag{19}$$

Expanding $C(\theta)$ in terms of the C_ℓ as above (18), we find

$$S_{1/2} = \sum_{\ell,\ell'} C_\ell \mathcal{I}_{\ell,\ell'} C_{\ell'}, \tag{20}$$

where

$$\mathcal{I}_{\ell,\ell'} \equiv \frac{(2\ell+1)(2\ell'+1)}{(4\pi)^2} \int_{-1/2}^{1} P_\ell(\cos\theta) P_{\ell'}(\cos\theta) \, \mathrm{d}(\cos\theta) \tag{21}$$

is a known matrix (see Copi et al. 2010) that can be evaluated.

The estimator generally employed for $S_{1/2}$ is

$$\hat{S}_{1/2} = \sum_{\ell,\ell'} \hat{C}_\ell \mathcal{I}_{\ell,\ell'} \hat{C}_{\ell'}. \tag{22}$$

Even with $\hat{C}_\ell$ itself an optimal, unbiased estimator of C_ℓ, this does *not* produce an optimal, unbiased estimator for $S_{1/2}$ (Pontzen & Peiris 2010). For the unbiased estimator (12), we have

$$
\begin{aligned}
\langle \hat{C}_\ell \hat{C}_{\ell'} \rangle &= \sum_{\bar{\ell},\bar{\ell}'} \mathbf{F}^{-1}_{\ell,\bar{\ell}} \mathbf{F}^{-1}_{\bar{\ell}',\ell'} \left\langle \boldsymbol{y}_{\bar{\ell}} \, \boldsymbol{y}_{\bar{\ell}'}{}^{\mathrm{T}} \right\rangle \\
&= \sum_{\bar{\ell},\bar{\ell}'} \mathbf{F}^{-1}_{\ell,\bar{\ell}} \mathbf{F}^{-1}_{\bar{\ell}',\ell'} \left(\langle \boldsymbol{y}_{\bar{\ell}} \rangle \langle \boldsymbol{y}_{\bar{\ell}'} \rangle^{\mathrm{T}} + \mathbf{F}_{\bar{\ell},\bar{\ell}'} \right) \\
&= \sum_{\bar{\ell}} \left(\sum_{\bar{\ell}'} \left\langle \mathbf{F}^{-1}_{\ell,\bar{\ell}} \boldsymbol{y}_{\bar{\ell}} \right\rangle \left\langle \mathbf{F}^{-1}_{\ell',\bar{\ell}'} \boldsymbol{y}_{\bar{\ell}'} \right\rangle^{\mathrm{T}} + \mathbf{F}^{-1}_{\ell,\bar{\ell}} \delta_{\ell',\bar{\ell}} \right) \\
&\approx C_\ell C_{\ell'} + \frac{2}{2\ell+1} C_\ell^2 \delta_{\ell,\ell'}. \tag{23}
\end{aligned}
$$

In the second line we have used the definition of the Fisher matrix (11), the third line is an algebraic simplification, and in the final line we have again used (12), the fact that $\hat{C}_\ell$ is unbiased, and the approximation from (13). With this, it now straightforward to see that

$$
\begin{aligned}
\langle \hat{S}_{1/2} \rangle &= \sum_{\ell,\ell'} \langle \hat{C}_\ell \hat{C}_{\ell'} \rangle \mathcal{I}_{\ell,\ell} = S_{1/2} + \sum_\ell \frac{2 C_\ell^2}{2\ell+1} \mathcal{I}_{\ell,\ell} \\
&\neq S_{1/2}. \tag{24}
\end{aligned}
$$

It is thus clear that (22) is a biased estimator and, in fact, is biased towards larger values of $S_{1/2}$.

As noted by Pontzen & Peiris (2010), this is of 'pedagogical interest' but does not affect the studies of low $S_{1/2}$. The Monte Carlo simulations employed (see Copi et al. 2009, for example) account for this bias. It does suggest that an alternative measure of the lack of large-angle correlations is desirable.

2.6 Assumptions

Efstathiou et al. (2010) claim that the full-sky, large-angle CMB can be reconstructed solely from the harmonic structure of the CMB outside the masked, Galactic region, and independent of the contents of the masked portion of the sky. We will demonstrate in what follows that this claim does not hold up to closer scrutiny.

It is clear that without assumptions regarding the harmonic structure inside the masked region nothing can be said about it. In principle, the low-ℓ harmonic structure inside the masked region could be anything, ranging from no power to large power or wild oscillations, making the full-sky reconstruction impossible.

Assuming a cosmological origin for the observed microwave signal outside the masked region, it seems reasonable to assume that it will be consistent with the signal inside the masked region. With that assumption, the harmonic structure outside the masked region can be extended into the masked region. For actual, full-sky maps, there is a further assumption: the region inside the mask is well enough determined and statistically close enough to the region outside the mask that it does not bias the reconstruction. This latter assumption turns out not to be true as we demonstrate below.

Note also that if the region inside the mask is trusted, then there is no need to perform either masking or the reconstruction at all; the full-sky map can be analysed directly. Therefore, validity of the stringent assumptions required for the reconstruction obviates the very need for the reconstruction.

When the reconstruction formalism described above is applied to actual data, further assumptions are implicit. In our development, we have assumed that the temperature fluctuations contain pure CMB signal. In practice, besides pixel noise (which we have not included as described above), the data may contain unknown foregrounds. To avoid contamination by foregrounds, it is common to analyse a foreground-cleaned map, such as the ILC map, and to mask the most contaminated regions of the sky. In following this approach, care must be taken not to reintroduce contamination in the data prior to reconstruction. As we will show below, the standard process of preparing data for reconstruction, in particular smoothing the full-sky map, violates this requirement.

3 RESULTS

To explore how data handling prior to reconstruction affects the results, we have performed a series of Monte Carlo simulations of ΛCDM based on reconstruction procedures suggested in the literature. We have employed the simplest best-fitting ΛCDM model from *WMAP* based solely on the *WMAP* data. This is model 'lcdm+sz+lens' with 'wmap7' data from the lambda site. Our results are insensitive to the exact details of the model since we are performing a theoretical study to examine relative differences between reconstructions and not performing parameter estimation. Our simulations are performed at $N_{\mathrm{side}} = 128$ unless otherwise noted, and we will focus on the reconstruction of a_{2m} and C_2. Further, our simulations only consider $\ell_{\mathrm{recon}} = 10$, reconstructed from the pixels outside the KQ75y7 mask provided by *WMAP* and degraded to the appropriate resolution, and use the data from the *WMAP* 7-year release.

A collection of realizations of the full sky is created as follows.

(i) Generate a random sky at $N_{\mathrm{side}} = 512$ from the best-fitting ΛCDM model.

(ii) Extract the a_{2m} and calculate the power in the quadrupole, denote this value by C_2.

(iii) Rescale the a_{2m} so that the C_2 in the map has a fixed value, for example rescale so that $C_2 = 100\,(\mu\mathrm{K})^2$ by replacing the a_{2m} with $a_{2m} \to a_{2m}\sqrt{100\,(\mu\mathrm{K})^2/C_2}$. Note that this does not change the phase structure of the a_{2m}.

(iv) Smooth the map with a $10°$ Gaussian beam, if desired.

(v) Degrade the map to the desired resolution ($N_{\mathrm{side}} = 128$ or 16).

(vi) Repeat the rescaling of the a_{2m} for each value of C_2 that we wish to consider. In our simulations, we consider $C_2 = 10$–$10^4\,(\mu\mathrm{K})^2$. This ensures that the same map realization is used with only the quadrupole power changed.

This procedure constitutes a single realization. The results in this work are based on at least 20 000 realizations.

Degrading masks requires an extra processing step. Pixels near mask boundaries turn from the usual 1 or 0 to denote inclusion or exclusion from the analysis, respectively, to fractional values. We redefine our degraded masks by setting all pixels with a value greater than 0.7 to 1 and all others to 0. For the KQ75y7 mask, this process leaves about 70 per cent of the pixels for analysis. To be precise, at $N_{\mathrm{side}} = 128$ this leaves 136 828 unmasked pixels and at $N_{\mathrm{side}} = 16$ there are 2157 pixels left.

A map with a modest angular resolution contains all the low-ℓ CMB information, so it may seem surprising that we employ $N_{\mathrm{side}} = 128$ in our studies. Instead, it is common in low-ℓ studies to employ a map at $N_{\mathrm{side}} = 16$, corresponding to pixels of approximately $3°$ in

size (see Efstathiou et al. 2010, for a recent example of this). The effects of the choice of resolution, the need for smoothing a map prior to analysis and the leaking of information this causes will now be explored.

3.1 Choice of map resolution

The study of large-angle, low-ℓ properties of the CMB appears naively not to require high-resolution maps. Maps degraded to the resolution corresponding to $N_{\text{side}} = 16$ are commonly employed (de Oliveira-Costa & Tegmark 2006; Efstathiou et al. 2010). When a map is degraded by averaging over pixels, high-frequency noise is introduced as may be seen in Figs 1 and 2. These figures show the reconstructed a_{2m} using the optimal, unbiased estimator from equation (7) for realizations with $C_2 = 100\,(\mu K)^2$. The solid, red lines (dashed, blue lines) show the 5th and 95th percentile lines from our realizations for the reconstructed real (imaginary) parts of each a_{2m}, using maps degraded to $N_{\text{side}} = 128$ (Fig. 1) and $N_{\text{side}} = 16$ (Fig. 2) and pixels outside the KQ75y7 mask. As expected from an unbiased estimator, the reconstructed values track the true values (Fig. 1). Further, we see that the a_{21} are best determined, and the a_{20} and a_{22} have larger variances due to the mask which produces greater admixture of ambiguous modes for these cases. However, for $N_{\text{side}} = 16$ (Fig. 2), we see that the reconstruction does not track the true values and is instead biased. This bias is due to the averaging done to degrade the maps and becomes more significant the more the map is degraded. From this, we conclude that the coupling of the small-scale modes to the large-scale modes caused by using maps with resolution that is too coarse can be at least partly responsible for reconstruction bias.
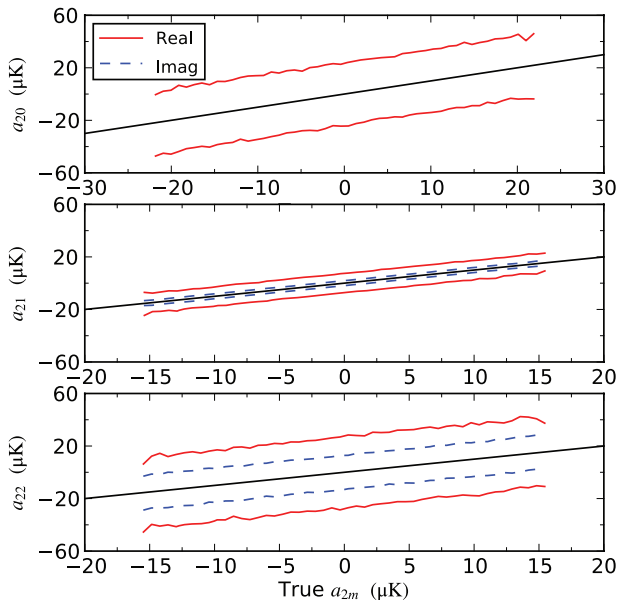

Figure 1. The 95th and 5th percentile lines for the a_{2m} reconstructed from the pixels outside the KQ75y7 mask at $N_{\text{side}} = 128$ (and thus $\ell_{\text{max}} = 514$) of ΛCDM realizations with $C_2 = 100\,(\mu K)^2$, as discussed in the text. The red, solid lines are for the real part of the a_{2m} and the blue, dashed lines are for the imaginary part. The black, solid line shows the expected result for a perfect reconstruction. We see that the reconstruction is unbiased, that is it tracks the true value.
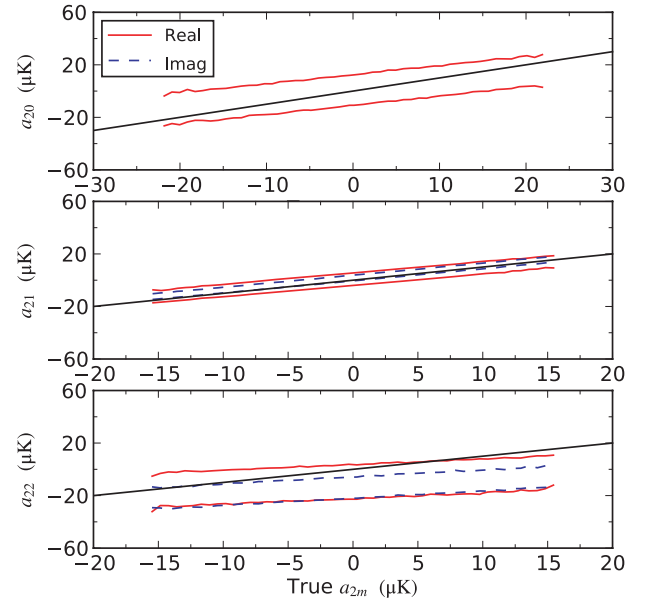
Figure 2. The same as Fig. 1, now reconstructed from the pixels outside the KQ75y7 mask at $N_{\text{side}} = 16$ (and thus $\ell_{\text{max}} = 66$). Here we see that the reconstruction is biased.

3.2 Smoothing the map

In practice, raw degraded maps are not used for the reasons shown in the previous section; instead, the maps are smoothed with a Gaussian beam with full width at half-maximum of at least the size of the pixels and then degraded. In this work, we employ a smoothing scale of $10°$, consistent with Efstathiou et al. (2010). Smoothing the maps studied in the previous section prior to reconstructing the $a_{\ell m}$ produces the results shown in Figs 3 and 4. With smoothing, we see that the $a_{\ell m}$ estimator is unbiased for both resolutions, $N_{\text{side}} = 128$ and 16. Smoothing is thus an essential step when working with low-resolution maps.
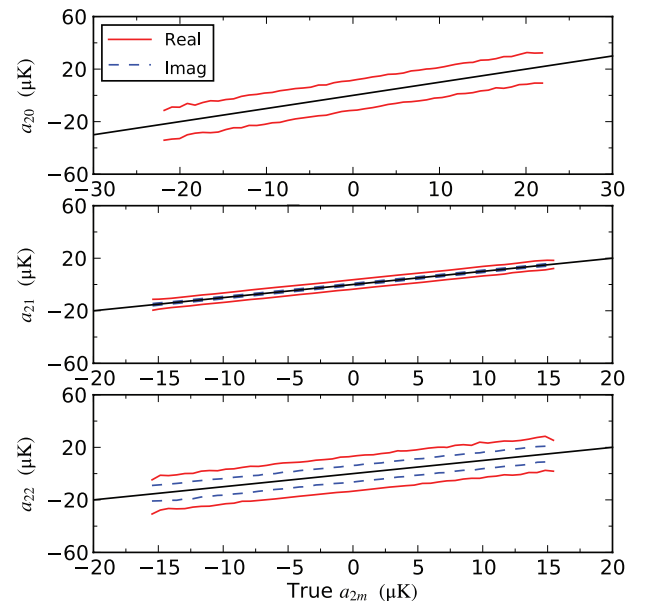

Figure 3. The same as Fig. 1, now reconstructed from maps smoothed with a $10°$ Gaussian beam applied to the full-sky map. As in Fig. 1, the reconstruction is unbiased.
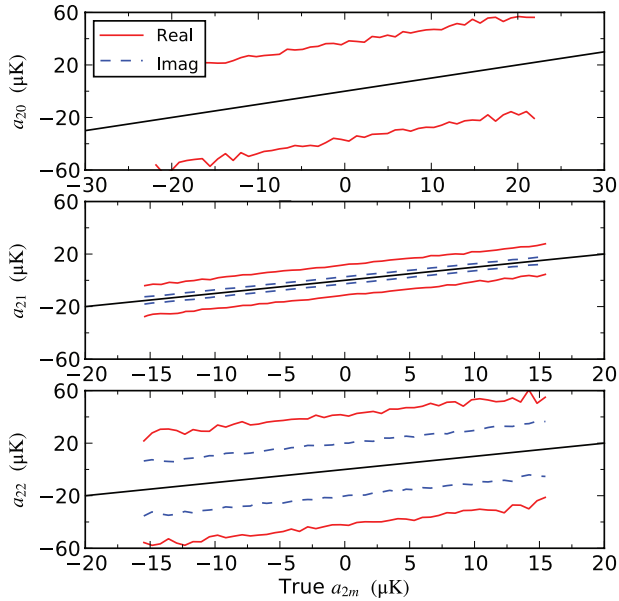
Figure 4. The same as Fig. 3, now reconstructed from maps with $N_{side} = 16$. The reconstruction is now also unbiased.

In Figs 3 and 4, we also see that the variance in the reconstructed values is resolution-dependent with the smaller variance provided by the higher resolution maps. Again this is not surprising, and can be understood as follows. Our covariance matrix in equation (8) does not include a noise term; yet, we have introduced noise by degrading. Smoothing does a good job at reducing the noise to a level where the reconstruction is unbiased; however, there is still residual noise that affects the covariance of the estimator. The higher the resolution, the smaller this noise. The best results are obtained by working at the highest resolution that is feasible. For this reason, we work at $N_{side} = 128$ in our simulations. See Appendix A for technical details.

3.3 Reconstructing the $a_{\ell m}$

We have now seen that the estimator in equation (7) is an optimal, unbiased estimator for the $a_{\ell m}$ when we work at high resolution and/or smooth the maps prior to reconstruction (Figs 1, 3 and 4). Although this has only been shown for $C_2 = 100 \, (\mu K)^2$, we have verified that this is true independent of the quadrupole power.

As noted above, the fact that we are smoothing the maps prior to masking imposes assumptions on the maps. For the realizations discussed above, the assumptions are met; the region inside the mask is, statistically, identical to the region outside. However, for real data the Galaxy is a bright foreground that must be removed. The *WMAP* ILC procedure attempts to do this and produce a full-sky CMB map. Even so, masking is often performed to avoid relying on the information inside this region since it may still be contaminated by Galactic foregrounds.

Unfortunately, when the map is smoothed, information leaks out of the masked region and biases the reconstruction as shown in Figs 5 and 6. For this analysis, for each synthetic map we filled the masked region with the corresponding portion (i.e. the masked region) taken from the ILC map. We then smoothed and degraded the resulting synthetic map. In these two figures, we show the true and reconstructed values of the coefficients a_{2m}; we also show the ILC map's a_{2m} for reference. We clearly see the bias in the reconstructed a_{2m} and its correlation with the ILC values. If $a_{2m}^{rec} < a_{2m}^{ILC}$, then a_{2m}^{rec} is
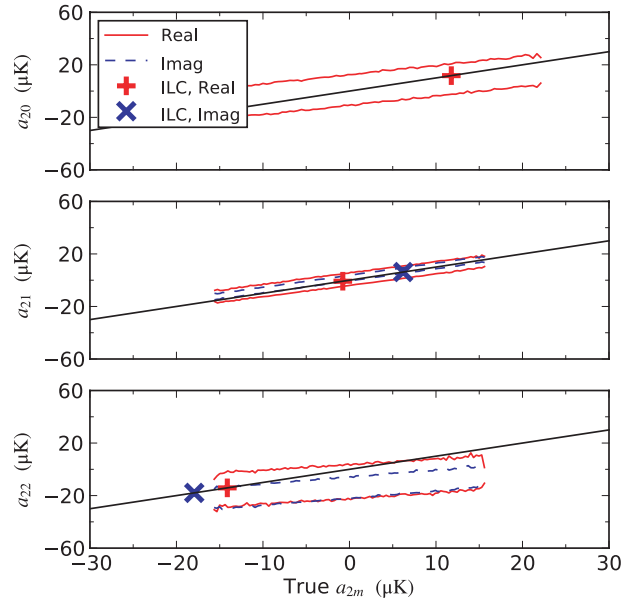

Figure 5. The same as Fig. 3, now with the masked region filled in with the ILC map *prior* to smoothing and rescaling. We clearly see that the reconstructed a_{2m} are *not* unbiased. The bias in reconstructing a_{20} and a_{22} is particularly apparent. This is due to the leakage of information from inside the masked region.
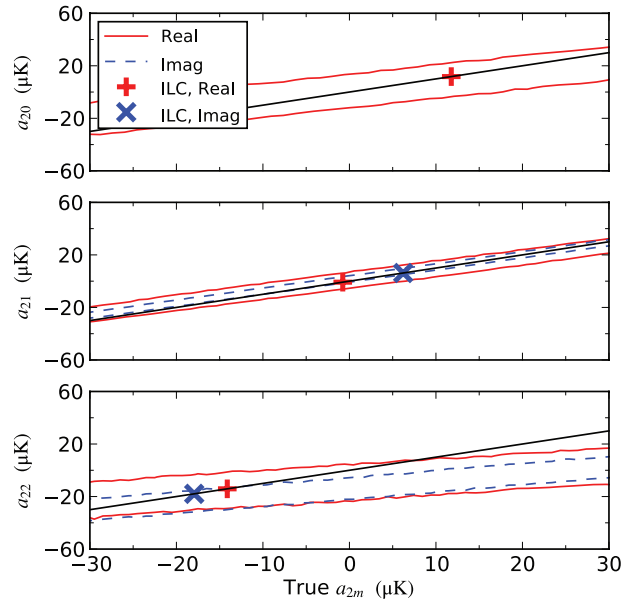

Figure 6. The same as Fig. 5, now with $C_2 = 1000 \, (\mu K)^2$.

biased upwards, and vice versa. For example, the ILC a_{22} values are large and negative, which leads to the reconstruction being skewed to agree better at large, negative values than at large positive values. This trend continues for the other a_{2m} and clearly shows that the smoothing has mixed information from the masked region.

We also recognize other details in the quality of the reconstruction that are specifically due to the orientation of the KQ75y7 mask in Galactic coordinates. For example, we see that the variance in the reconstructed real part of a_{22} is larger than that for the imaginary part of a_{22}; the reason is that the real part of Y_{22} has an extremum in the centre of the Milky Way where the mask 'bulges',

while the imaginary part has a node at this location. Therefore, more information relevant to the real part of a_{22} is missing than for the imaginary part, and the former has a larger reconstruction error. Moreover, it is also the case that the Y_{20} and Y_{22} have extrema in the Galactic plane, whereas Y_{21} has nodes. Due to this, the variances of a_{20} and a_{22} are expected to be larger than that of a_{21}, as our reconstruction plots show.

Note also that the reconstruction bias we find is *not* an artefact of the sharp transition introduced in the process of filling the masked regions of simulated maps with the ILC contents. The smoothing procedure, for one, completely removes the sharp feature in the map. Moreover, we have explicitly checked that the reconstructed $a_{\ell m}$ are not biased when the cut is filled with contents of *another* statistically isotropic map. Therefore, the reconstruction bias seen in our plots is real, and is caused to the specific structure of the ILC map behind the Galactic plane which 'leaks' into the unmasked region.

The question, then, is how to fill the masked region before smoothing. In principle, anything could be used to fill the Galactic region, but then the information about this fill would leak outside the mask due to the smoothing. If the map were masked prior to smoothing, then 'zero' would be leaked and bias the reconstruction. Alternatively, if the Galactic region were filled with Gaussian noise with rms value consistent with the region outside the Galaxy, then the estimator would be unbiased similar to the results in Fig. 1, but this would rely on the *assumption* that the true CMB inside the mask has precisely the same statistical properties as the CMB in the region outside. Filling with the ILC values would make sense if we could be completely confident that the ILC reconstruction of the region inside the mask is accurate. However, in the ILC the region inside the Galactic mask has different statistical properties than the region outside, particularly for the large-angle behaviour. This alone raises concerns that the ILC reconstruction is not entirely accurate. Further, if we knew how to properly treat the region inside the mask, either by accepting the ILC values or filling it with appropriate statistical values, there would be no need for a reconstruction as we would have a full-sky map to analyse!

The challenge is that there is no, or at least no unique, compelling choice of how to fill the masked region before smoothing. In the face of this, the approach we take below is to study how the admixture of the large-angle behaviour of the Galactic region from the ILC map affects the reconstruction of the low-ℓ CMB, particularly when the region outside the Galaxy has low quadrupole power and lack of large-angle correlations. We show how this particular choice biases the reconstruction.

3.4 Reconstructing the C_ℓ

Since we are interested in reconstructing $C(\theta)$, we next need to reconstruct the C_ℓ. From the $a_{\ell m}$, we first proceed using the naive estimator (16), denoted C_ℓ^e (as used to generate fig. 5 of Efstathiou et al. 2010).

The results for this estimator are shown in Fig. 7. For these realizations, the maps were *not* smoothed. The reconstruction is shown as the dashed, red lines representing the 5th, 50th and 95th percentile values as a function of the true C_2 used to generate the maps. The solid, blue lines are the equivalent values from the reconstruction based on the pixel estimator from SPICE. Again the solid, black line is the reconstructed true relation plotted to guide the eye. At large C_2, we see the desired behaviour: the reconstructed values from both estimators are centred around the true value, and C_2^e does have a smaller variance, as an optimal estimator should
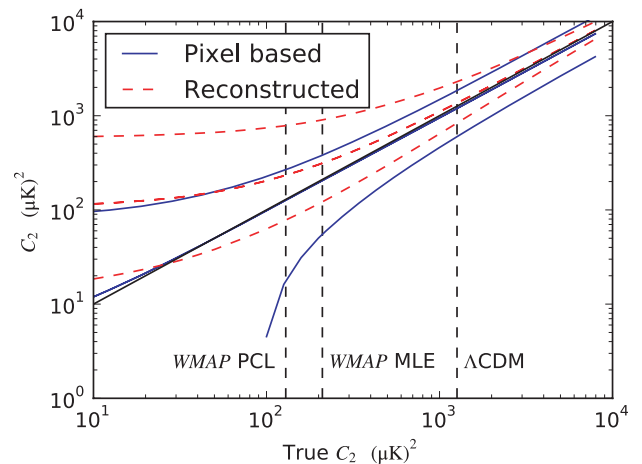

Figure 7. The 95th, 50th and 5th percentile lines of the reconstructed C_2 (top to bottom, respectively) from our realizations. The maps have *not* been smoothed prior to reconstruction. The pixel based (blue, solid line) comes from SPICE, whereas the reconstructed (red, dashed line) is the estimator C_ℓ^e. We see that this estimator is clearly biased towards larger reconstructed values for small, true C_2, such as the values extracted from *WMAP* using either the PCL or MLE procedures. For a value of C_2 near the ΛCDM value, the reconstruction method is a good estimator. The pixel-based method produces values of C_2 with a median much closer to the true values, though with larger error bars.

(however, this does not mean it *is* optimal). At low C_2, in particular near the *WMAP* PCL and MLE values, the pixel-based estimator is still centred around the true value, though with large variance; however, the C_2^e is now biased towards larger values.

The results in Fig. 7 were for unsmoothed maps. The usual approach is to smooth the maps, which suppresses power on small scales (high ℓ). Fig. 8 shows the results when the maps are smoothed prior to reconstruction; they are encouraging. Both estimators now track the true values much more closely. Even the median of C_2^e remains close to the true value for values near the *WMAP* PCL value. This shows that with smoothing the correlations are reduced due to the lack of high-frequency noise. It suggests that smoothing the map, reconstructing the $a_{\ell m}$ and employing C_ℓ^e as our estimator are sufficient and nearly optimal.
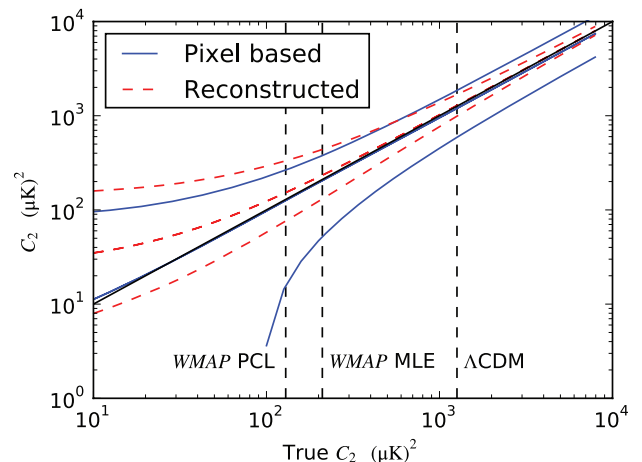

Figure 8. The same as Fig. 7, now with the realizations smoothed to $10°$ prior to reconstruction. It appears that the estimator (16) does a better job of reproducing C_2 for a ΛCDM model, though see Fig. 9.
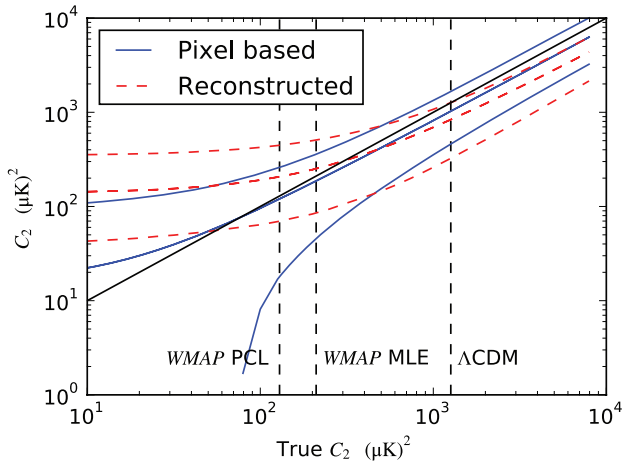
Figure 9. The same as Fig. 8, now with the region inside the masked region replaced by the ILC prior to smoothing to 10° and reconstructing. Clearly, the ILC information from inside the masked region has leaked out, biasing the reconstruction. Not surprisingly, the reconstruction now is only accurate near the *WMAP* MLE value, the value consistent with this region of the ILC. At lower C_2 values, the reconstruction plateaus to this value as it is the main contribution to quadrupole power. At higher values of C_2, the quadrupole power is suppressed by the leakage.

Unfortunately this is not the case. As noted above, smoothing makes assumptions about the validity of the region inside the mask. We saw that even for the $a_{\ell m}$ this leads to a bias (see Fig. 5). When the corresponding ILC portion is placed into the masked region prior to smoothing, the C_2^e is also biased as shown in Fig. 9. We see that the masked region drives C_2^e to be near the value inside the mask (approximately the *WMAP* MLE value). The C_2^e results are biased upwards for very small C_2 and downwards for large C_2. Thus, even though smoothing helps in removing the correlation bias in the C_ℓ^e estimator, it introduces its own bias. How the masked region is filled determines how the distribution of C_2^e–C_2^{true} will be skewed. Roughly speaking, the values inside the mask will be favoured, raising the reconstructed values that are lower than the masked region values, and lowering values that are higher than those from the masked region.

We have seen that the naive estimator, C_ℓ^e, provides an unbiased estimate of C_2 when the true value is near the expected, ΛCDM value. However, when the true value is low, this estimator tends to *overestimate* C_2. Further, when smoothing is applied, the reconstruction skews the values towards those consistent with the region inside the mask. This is to be expected. In fact, if the region inside the mask were believed, then there would be no need to reconstruct at all; a full-sky map would already exist and it could be used for analysis without this extra effort.

3.5 Optimal, unbiased C_ℓ estimator

The general behaviour found for the naive estimator, C_ℓ^e, carries over to the optimal, unbiased estimator, $\hat{C}_\ell$, based on the weighted harmonic coefficients (12), as we now see. Calculating $\hat{C}_\ell$ for the realizations considered above, we find the results in Fig. 10 for Gaussian-smoothed maps. This figure should be compared to Fig. 8. We see that $\hat{C}_2$ is nearly unbiased over the full range of true C_2 as expected.

The effect of smoothing when the ILC is inserted into the masked region is shown in Fig. 11. Again we see the bias introduced by smoothing when the two regions do not contain the same structure.
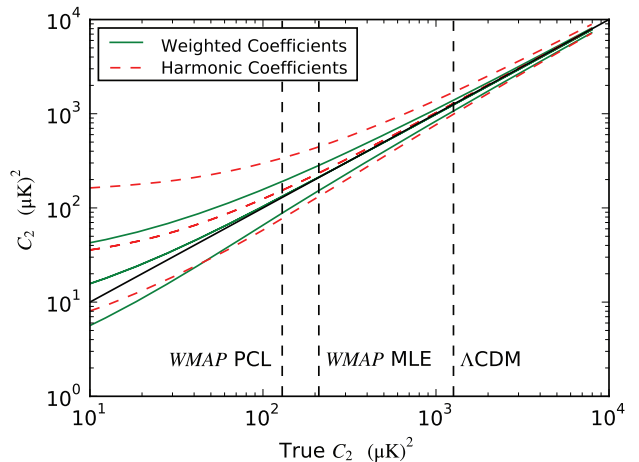

Figure 10. Similar to Fig. 8, now comparing C_2^e, the harmonic coefficient estimator (16) again as the dashed, red lines to $\hat{C}_2$, the weighted harmonic coefficient estimator (12) as the green, solid lines. We see that the weighted harmonic coefficient estimator is unbiased over the full true C_2 range.
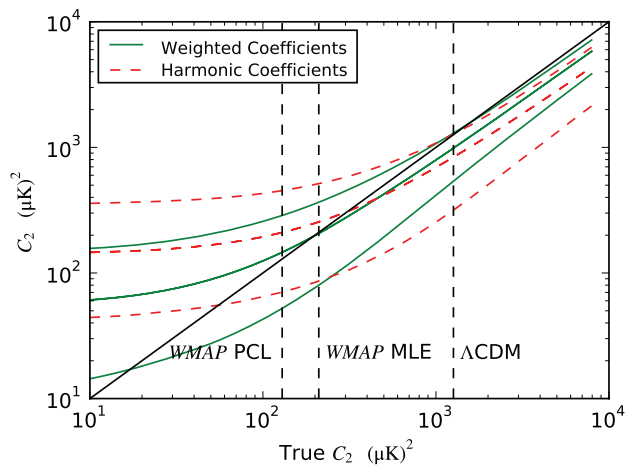

Figure 11. The same as Fig. 10, now for the Galactic region filled with the ILC values. We see that both estimators are now biased to agree best near the *WMAP* MLE value as we saw in Fig. 9.

These results are qualitatively similar to those found in Fig. 9 and the same discussion applies.

3.6 Reconstructing without smoothing

The reconstruction of the a_{2m} without smoothing showed that for $N_{\text{side}} = 128$ the reconstruction was unbiased (Fig. 1) but for $N_{\text{side}} = 16$ there was a resolution-dependent bias (Fig. 2). Calculating the weighted harmonic coefficient estimator (12) from these realizations produces the results in Fig. 12. At first glance, these results are surprising and encouraging. The green, solid lines for $N_{\text{side}} = 128$ and red, dashed lines for $N_{\text{side}} = 16$ nearly overlap and the central value very closely follows the true value. This is surprising since the a_{2m} at $N_{\text{side}} = 16$ are biased and have smaller variance than the corresponding $N_{\text{side}} = 128$ (see Figs 1 and 2). Even so, when combined to determine C_2, these differences average out and lead to nearly identical predictions.

Based on Fig. 12, we may think we have solved the reconstruction problem; just reconstruct using the optimal, unbiased C_ℓ estimator (12) without smoothing! Unfortunately, we cannot draw this

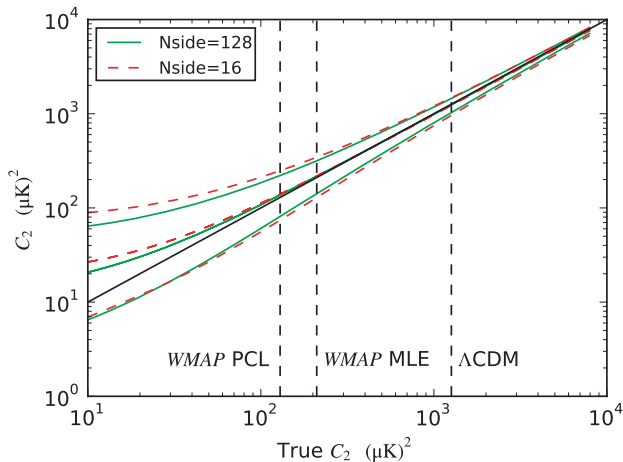**Figure 12.** The same as Fig. 10, now comparing the weighted harmonic coefficient estimator (12) for $N_{side} = 128$ as the green, solid lines and $N_{side} = 16$ as the red, dashed lines without smoothing the map prior to reconstruction. Since there is no smoothing, the results do not depend on the contents of the masked galactic region. We see that the reconstruction without smoothing is unbiased for most of the C_2 range, however see Section 3.6 for a discussion of its inapplicability to real data.

Table 1. $S_{1/2}$ values for the ILC map calculated for $2 \leq \ell \leq 10$. The map is unprocessed, Gaussian-smoothed with a $10°$ beam, or had the Galactic region filled with a Gaussian random, statistically isotropic sky realization with the same power spectrum as the region outside this region prior to smoothing. The values are calculated for the full sky and for the KQ75y7 masked sky at $N_{side} = 128$ using a pixel-based estimator or the optimal, unbiased C_ℓ estimator (12) from maps at $N_{side} = 128$ and 16. The last row refers to the map whose mask area has been filled with Gaussian random field whose power is consistent with power measured outside the mask.

ILC map processing	$S_{1/2}$ ($\mu K)^4$			
	Full sky	Cut sky pixel-based	Reconstructed sky	
			N_{side} =128	N_{side} =16
Unsmoothed	8835	1275	5390	2300
$10°$ smoothing	8835	1270	2230	1670
Filled with consistent power and smoothed	1020	1290	1020	950

in each ℓ-mode as the region outside the mask but with the phases randomized.

The results in Table 1 are consistent with what we have found for the C_ℓ reconstructions. For the unsmoothed map, the full-sky and pixel-based estimators calculated at $N_{side} = 128$ show the usual result, the large discrepancy between the full and cut-sky values. This holds true for the smoothed map also. Further, the reconstructed values show the large discrepancy between the unsmoothed and smoothed maps (see, for example, Figs 2 and 4). We also see that the reconstructed values are systematically larger than the pixel-based estimator showing that the reconstruction is more sensitive to leakage for information from inside the masked region. Finally, the last line of the table shows the expected behaviour for a map where the full sky has power consistent with that from the cut sky. Note that the cut-sky pixel-based results are consistent with each other since information leakage is unimportant. The small difference between the $N_{side} = 128$ and 16 reconstructions shows the residual sensitivity on resolution.

conclusion from the results presented here. Recall that the reconstructions have been performed on noise-free, pure CMB maps. Real maps contain noise and potentially residual, unmasked foregrounds. In particular, uncorrected, diffuse foregrounds are known to contaminate the low-ℓ reconstruction (Naselsky et al. 2008). A careful study of the issues faced when applying the reconstruction to real data is beyond the scope of this work and will be reserved for future study. However, naive application of this method to real data yields highly biased reconstructions.

3.7 $S_{1/2}$ estimator

The study of the $S_{1/2}$ statistic is a large project in its own right and will not be pursued in detail here. Our Universe as encoded in the ILC map contains a somewhat small full-sky $S_{1/2}$ and an extremely small cut sky $S_{1/2}$. If we are to perform such a statistical study of $S_{1/2}$, we could enforce this structure, that is only choose skies that have somewhat low full sky and very low cut-sky $S_{1/2}$ values. Alternatively, we could choose from an ensemble based on the best-fitting ΛCDM model. In the latter case, it has already been shown that the ILC map is a rare realization, unlikely at the 99.975 per cent level (Copi et al. 2009). The assumptions made in any study will determine the statistical questions that can be asked. Conversely, the statistical questions asked will implicitly contain the assumptions imposed.

In Table 1, we show the $S_{1/2}$ for the ILC map calculated from (22) under various assumptions. Note that these values all contain the bias discussed in Section 2.5 as is standard in the literature. Shown in the table are the values calculated for the full sky and for the partial sky where the KQ75y7 mask is employed to cut out the Galactic region. The cut-sky results are calculated using the pixel-based estimator of SPICE and the optimal, unbiased C_ℓ estimator (12) from reconstructed maps at $N_{side} = 128$ and 16. Further, the results are shown for different map processing, including no processing (the unsmoothed entry where the map has only been degraded as required for the reconstruction), employing a $10°$ Gaussian smoothing, and filling the Galactic region with a realization that has the same power

3.8 Higher multipoles

In this work, we have focused on how data handling affects the reconstruction of the quadrupole. The quadrupole serves as an example of the general behaviour. As shown in Figs 13 and 14, we see the same results for $\ell = 3$ and 4. These figures were generated from the same realizations employed in making Fig. 5. Again we see that the reconstruction is biased towards the values from the ILC map.

4 CONCLUSIONS

It has been argued that the large-angle CMB can be reliably reconstructed from partial-sky data and that when this is done the lack of large-angle correlation is not significantly deviant from the expectation (Efstathiou et al. 2010). At first glance the argument appears sound. The large-angle modes extend over large fractions of the sky; thus, knowing their values on one region of the sky allows us to extrapolate them into the masked regions. However, in practice and under close scrutiny, this argument fails. Implicit assumptions built in to the reconstruction process enforce agreement between the reconstruction and the previously constructed full sky (the ILC map in this case) through mixing of information from inside the masked region to that outside. Due to this, the reconstruction has no
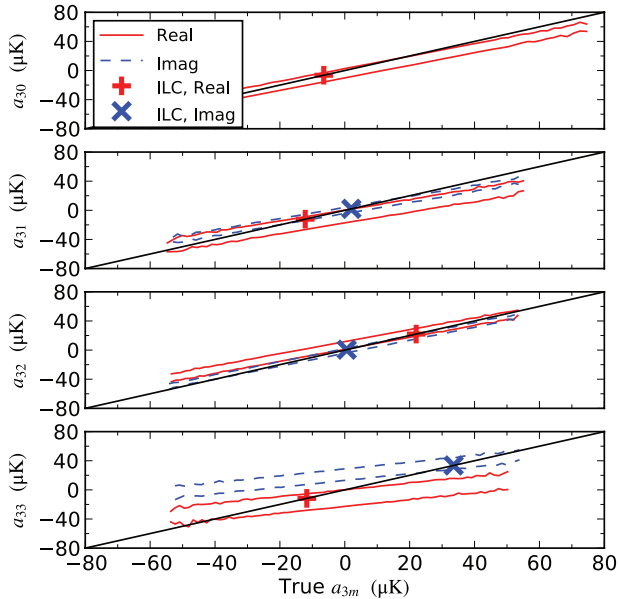
Figure 13. The 95th and 5th percentile lines for the a_{3m} reconstructed from the pixels outside the KQ75y7 mask at $N_{\mathrm{side}} = 128$ (and thus $\ell_{\max} = 514$) of ΛCDM realizations with $C_2 = 100\,(\mu\mathrm{K})^2$ and the masked region filled in with the ILC map *prior* to smoothing and rescaling, as discussed in the text. The red, solid lines are for the real part of the a_{3m} and the blue, dashed lines are for the imaginary part. The black, solid line shows the expected result for a perfect reconstruction. We clearly see that the reconstructed a_{3m} are *not* unbiased. Now the bias is most prominent for a_{33}, the octopole mode with all its extrema within the Galactic plane. This figure should be compared to Fig. 5.
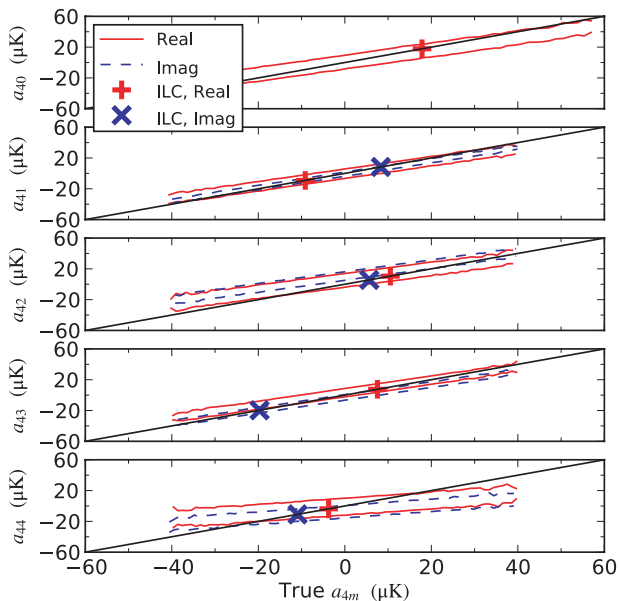

Figure 14. The same as Fig. 13, now for $\ell = 4$.

value independent of the original full-sky map. It neither confirms nor denies the validity of that map.

To study the large-angle CMB, a choice must be made on what data to take as a fair representation of the CMB sky. One choice is to accept a cleaned, full-sky map, such as the ILC map produced by *WMAP*, to accurately represent the primordial CMB sky. In this case, the full-sky map may be analysed with no reconstruction required.

In Copi et al. (2009) and in this work, however, we have taken the region outside the Galaxy as defined by the *WMAP* KQ75y7 mask to be a fair representation. We have shown that the large-angle CMB can be reconstructed using unbiased estimators for the $a_{\ell m}$ and C_ℓ; however, the standard approach requires processing the original map by degrading and smoothing it. Unfortunately, it is precisely the smoothing process that mixes the region we have taken as a fair representation of the CMB with the region we are trying to exclude. When the excluded region has the same statistical properties as the region we are including, no biases are introduced. On the other hand, when, as is the case with the ILC map, the properties are significantly different, the reconstruction is biased to agree with the full map. This is not surprising. Through this process one is trusting the full-sky map, mixing information from it into the rest of the sky, then reconstructing it. This is a circular process and is unnecessary. If the full-sky map is already trusted, then there is no point in performing a reconstruction to produce a poorer version of the original map.

The important point is that even *in principle* reconstructing following the standard approach leads to biased results unless the full-sky CMB is already known. We have shown for noise-free, pure CMB maps that smoothing mixes information and biases the results. When applied to real data, the problems only get worse. Encouragingly, we also found that *in principle* reconstructing without smoothing leads to unbiased results. Unfortunately, directly applying this to real data with noise and residual, unmasked foregrounds yields highly biased reconstructions requiring further care to apply this method successfully to real-world CMB.

Overall, the question of how to perform an unbiased reconstruction of the full large-angle CMB sky remains an interesting one. Previous work (Bielewicz et al. 2004; Naselsky et al. 2008; Liu & Li 2009; Aurich & Lustig 2011) has shown that contamination significantly affects the reconstruction of the large-angle multipole moments. Aurich & Lustig (2011) studied the case most similar to that considered in this work. They showed that smoothing of full-sky map leaks information from the pixels not used in the reconstruction (those in a mask) to the pixels that will be used. In this work, we have extended their result and shown how a reconstruction such as that performed by Efstathiou et al. (2010) is biased due to this leakage of information. This shows the fundamental problem in trying to reconstruct the full sky from a partial sky.

Fortunately, large-angle CMB studies are not dependent on reconstructed full-sky maps. The partial sky when used consistently (see Copi et al. 2009, for example) has been shown to be a robust representation of the large-scale CMB by Aurich & Lustig (2011) and in this work. Despite the fact that such an approach is suboptimal in the sense that the inferred C_ℓ do not have the smallest possible variance, it is far less biased than the 'optimal' C_ℓ inferred through the maximum-likelihood reconstruction. More robust statements about the large-angle CMB behaviour may therefore be made with the partial-sky pixel-based C_ℓ.

We conclude that the lack of large-angle correlation, particularly on the region of the sky outside the Galaxy, remains a matter of serious concern.

REFERENCES

Afshordi N., Geshnizjani G., Khoury J., 2009, J. Cosmol. Astropart. Phys., 8, 30

Aurich R., Lustig S., 2011, MNRAS, 411, 124

Bennett C. L. et al., 1996, ApJ, 464, L1

Bennett C. L. et al., 2003, ApJS, 148, 1

Bennett C. L. et al., 2011, ApJS, 192, 17

Bielewicz P., Górski K. M., Banday A. J., 2004, MNRAS, 355, 1283

Chon G., Challinor A., Prunet S., Hivon E., Szapudi I., 2004, MNRAS, 350, 914

Copi C. J., Huterer D., Schwarz D. J., Starkman G. D., 2006, MNRAS, 367, 79

Copi C. J., Huterer D., Schwarz D. J., Starkman G. D., 2007, Phys. Rev. D, 75, 023507

Copi C. J., Huterer D., Schwarz D. J., Starkman G. D., 2009, MNRAS, 399, 295

Copi C. J., Huterer D., Schwarz D. J., Starkman G. D., 2010, Advances Astron., 2010, 78

de Oliveira-Costa A., Tegmark M., 2006, Phys. Rev. D, 74, 023005

de Oliveira-Costa A., Tegmark M., Zaldarriaga M., Hamilton A., 2004, Phys. Rev. D, 69, 063516

Efstathiou G., 2004, MNRAS, 349, 603

Efstathiou G., Ma Y., Hanson D., 2010, MNRAS, 407, 2530

Eriksen H. K., Hansen F. K., Banday A. J., Górski K. M., Lilje P. B., 2004a, ApJ, 605, 14

Eriksen H. K., Hansen F. K., Banday A. J., Górski K. M., Lilje P. B., 2004b, ApJ, 609, 1198

Górski K. M., Hivon E., Banday A. J., Wandelt B. D., Hansen F. K., Reinecke M., Bartelmann M., 2005, ApJ, 622, 759

Hajian A., 2007, preprint (astro-ph/0702723)

Hansen F. K., Banday A. J., Górski K. M., Eriksen H. K., Lilje P. B., 2009, ApJ, 704, 1448

Kim J., Naselsky P., 2010a, ApJ, 714, L265

Kim J., Naselsky P., 2010b, Phys. Rev. D, 82, 063002

Kim J., Naselsky P., 2010c, preprint (arXiv:1011.0377)

Kim J., Naselsky P., 2010d, ApJ, 724, L217

Land K., Magueijo J., 2005, MNRAS, 362, 838

Larson D. et al., 2011, ApJS, 192, 16

Liu H., Li T., 2009, Sci. China G: Phys. Astron., 52, 804

Naselsky P. D., Verkhodanov O. V., Nielsen M. T. B., 2008, Astrophys. Bull., 63, 216

Pontzen A., Peiris H. V., 2010, Phys. Rev. D, 81, 103008

Press W. H., Teukolsky S. A., Vetterling W. T., Flannery B. P., 1992, Numerical Recipes in C, 2nd edn. Cambridge Univ. Press, Cambridge

Sarkar D., Huterer D., Copi C. J., Starkman G. D., Schwarz D. J., 2011, Astropart. Phys., 34, 591

Schwarz D. J., Starkman G. D., Huterer D., Copi C. J., 2004, Phys. Rev. Lett., 93, 221301

Slosar A., Seljak U., 2004, Phys. Rev. D, 70, 083002

Spergel D. N. et al., 2003, ApJS, 148, 175

Tegmark M., 1997, Phys. Rev. D, 55, 5895

APPENDIX A: RECONSTRUCTING AT HIGH RESOLUTION

Computationally, the time and memory intensive step in reconstructing $a_{\ell m}$ and C_ℓ from our estimators (7) and (12) is the inversion of the covariance matrix, $\mathbf{C}$. Fortunately, this step only needs to be performed once for each choice of resolution, N_{side}, and mask.

The covariance matrix is of size $N_{\text{pix}} \times N_{\text{pix}}$, where the number of pixels is given by $12(N_{\text{side}})^2$ and the size of $\mathbf{C}$ scales as $(N_{\text{side}})^4$. An increase in resolution by one step, $N_{\text{side}} \to 2N_{\text{side}}$, increases the size of $\mathbf{C}$ by a factor of 16. Working with cut skies does not appreciably reduce this; even the largest mask, KQ75y7, only cuts out 25–30 per cent of the pixels. Resolutions of $N_{\text{side}} = 32$ or perhaps even $N_{\text{side}} = 64$ are attainable on a desktop computer. Fortunately, we never need to store the full $\mathbf{C}^{-1}$ and can calculate the elements of $\mathbf{C}$ as required instead of storing them.

In our estimators, all the matrices that we encounter, except for $\mathbf{C}^{-1}$, are of size $N_\ell \times N_{\text{pix}}$ or smaller. Here $N_\ell = (\ell_{\text{recon}} + 1)^2$. Even for $N_{\text{side}} = 512$ and $\ell_{\text{recon}} = 10$ these matrices only require about 3 GB of storage at double precision. Further, we see that only the matrix

$$\mathbf{M} \equiv \mathbf{C}^{-1}\mathbf{Y} \tag{A1}$$

is ever required (see equations 7 and 8).

To compute $\mathbf{M}$ we note that it satisfies the set of linear equations

$$\mathbf{CM} = \mathbf{CC}^{-1}\mathbf{Y} = \mathbf{Y}. \tag{A2}$$

Solving such a set of equations is a standard problem in computational linear algebra. A covariance matrix is symmetric and positive-definite, so it may be factored with a Cholesky decomposition (Press et al. 1992)

$$\mathbf{C} = \mathbf{LL}^{\text{T}}, \tag{A3}$$

where $\mathbf{L}$ is a lower triangular matrix. Our problem then becomes solving

$$\mathbf{L}(\mathbf{L}^{\text{T}}\mathbf{M}) \equiv \mathbf{Lz} = \mathbf{Y}. \tag{A4}$$

This can be solved in two steps using backward substitution on $\mathbf{Lz} = \mathbf{Y}$ to find $\mathbf{z}$ followed by forward substitution on $\mathbf{L}^{\text{T}}\mathbf{M} = \mathbf{z}$ to find $\mathbf{M}$.

At this point we are left with computing $\mathbf{L}$. Approximately half of this matrix is zero, so only half of it needs to be stored (of course the same is true of $\mathbf{C}$ since it is symmetric). Unfortunately, this cannot be further reduced and this provides the limiting factor in determining the resolution at which we can work. For $N_{\text{side}} = 128$ and $\ell_{\text{recon}} = 10$, the matrix $\mathbf{L}$ is approximately 70 GB in size. Improving resolution to $N_{\text{side}} = 256$ increases the required storage to over 1 TB. This is what has limited our work to $N_{\text{side}} = 128$. Straightforward, numerically stable algorithms exist for calculating $\mathbf{L}$ (see Press et al. 1992, for example). Though this is a time-consuming step, once $\mathbf{M}$ is calculated the rest follows quickly.

This paper has been typeset from a TEX/LATEX file prepared by the author.